

# CdSe–CdS Nanoheteroplatelets with Efficient Photoexcitation of Central CdSe Region through Epitaxially Grown CdS Wings

Anatol Prudnikau,<sup>†</sup> Andrey Chuvilin,<sup>‡,§</sup> and Mikhail Artemyev<sup>\*,†</sup>

<sup>†</sup>Institute for Physico-Chemical Problems, Belarusian State University, Leningradskaya str., 14, Minsk 220030, Belarus

<sup>‡</sup>CIC nanoGUNE, Tolosa Hiribidea, 76, E-20018 Donostia-San Sebastian, Spain

<sup>§</sup>IKERBASQUE, Basque Foundation for Science, 48011 Bilbao, Spain

## Supporting Information

**ABSTRACT:** We synthesized a new type of optically active semiconductor nanoheterostructure based on CdSe nanoplatelets with epitaxially grown CdS flat branches or wings. CdS branches work as efficient photonic antenna in the blue spectral region, enhancing the excitation of CdSe band edge emission. The formation of CdSe–CdS nanoheteroplatelets instead of CdSe/CdS core–shell nanoplatelets was achieved using short-chain Cd ethylhexanoate and sulfur in octadecene as precursors for CdS overgrowth in the presence of acetate salt.

Recently discovered colloidal CdSe nanoplatelets (NPLs) represent a new type of two-dimensional (2D) semiconductor nanocrystals and show strong one-dimensional (1D) quantum confinement.<sup>1–8</sup> Together with zero-dimensional quantum dots (QDs) and 1D nanorods (NRs), the 2D NPLs complete the family of quantum-confined semiconductor nanocrystals. CdSe NPLs possess unique optical properties which make them suitable for practical applications. As compared with CdSe QDs and NRs, the NPLs show much narrower excitonic optical absorption and photoluminescence (PL) bands, which is important in fabrication of monochromatic light-emitting devices. The flat geometry and very large surface area of NPLs are useful parameters for photovoltaic structures and optical chemical sensors. The average lateral dimension of reported CdSe NPLs was in the range of ca.  $20 \times 20 \text{ nm}^2$  and the thickness 2–6 CdSe monolayers (ML). The lateral shape of the NPLs may vary from square to rectangular, and very large NPLs may roll into CdSe nanotubes. The general route for colloidal synthesis of CdSe NPLs includes the pre-formation of ultrasmall CdSe seeds followed by their recrystallization or growth in the presence of acetate ions (cadmium or zinc acetate, etc.).

Practical application of colloidal semiconductor nanocrystals usually requires capping of the core CdSe QDs or NRs with wide-gap materials, like CdS or ZnS. The wide-gap epitaxial shell creates an appropriate potential barrier for photoexcited electron–hole pairs and protects the core from chemical interactions with surrounding media, giving increased photostability and chemical stability and high PL quantum yield. The same is true for CdSe NPLs, too, especially considering their intrinsically higher sensitivity to the chemical environment due to their extremely high surface area. The usual procedure for CdS shell growth atop a CdSe core is based on simultaneous or

sequential introduction of Cd and sulfur-containing precursors into the reaction mixture with CdSe core nanoparticles. Recently, a sequential variant was successfully realized using Cd acetate and bis(trimethylsilyl) sulfide or  $(\text{NH}_4)_2\text{S}$  as precursors for sulfur, resulting in nearly perfect CdSe/CdS core–shell NPLs.<sup>9,10</sup> Here, we show that a similar reaction may result in the formation of CdSe–CdS nanoheteroplatelets with CdS grown as flat branches at the edges of the CdSe core.

The 5 ML CdSe NPLs with ca.  $10 \text{ nm} \times 30 \text{ nm}$  lateral size were synthesized by a modification of the protocol described in refs 4 and 5. Our NPLs have a narrow PL band centered at about 512 nm, in full compliance with other reports. CdSe core NPLs were overgrown with CdS in octadecene solution containing cadmium acetate and oleic acid for better solubility and stabilization of the flat geometry of nanoparticles. Cadmium ethylhexanoate and elemental sulfur dissolved in octadecene were used as precursors for CdS growth (details of the synthesis can be found in the Supporting Information). Periodically, aliquots of colloidal solution of growing nanocrystals were withdrawn by syringe and diluted with chloroform in a 1 cm quartz optical cuvette. The optical absorption, room-temperature PL, and PL excitation (PLE) spectra were registered immediately after the dilution. Simultaneously, a portion of the same nanocrystals purified by multiple deposition/redispersion procedures was placed on a copper grid for TEM measurements.

Figure 1 shows optical absorption, PL, and PLE spectra of colloidal solutions of CdSe NPLs at different CdS overgrowth times. The PLE spectrum in Figure 1a (blue curve) follows well the absorption spectrum (black curve) of bare CdSe NPLs. We registered a PLE spectrum at the red side of the PL band ( $\lambda_{\text{em}} = 525 \text{ nm}$ ) in order to compare the positions of the first excitonic resonance in absorption and PLE spectra. After addition of one-third of the Cd and S precursors, the PL spectrum remained unchanged (red curve in Figure 1b), while a new peak at 410 nm appeared in the absorption spectrum and grew in amplitude with further addition of Cd and S precursors (black curves in Figure 1b,c). We did not observe any additional PL peaks associated with this new optical transition. Moreover, as can be seen from Figure 1c, the PLE spectrum follows the corresponding absorption spectrum, which points to the

Received: February 17, 2013

Published: September 18, 2013

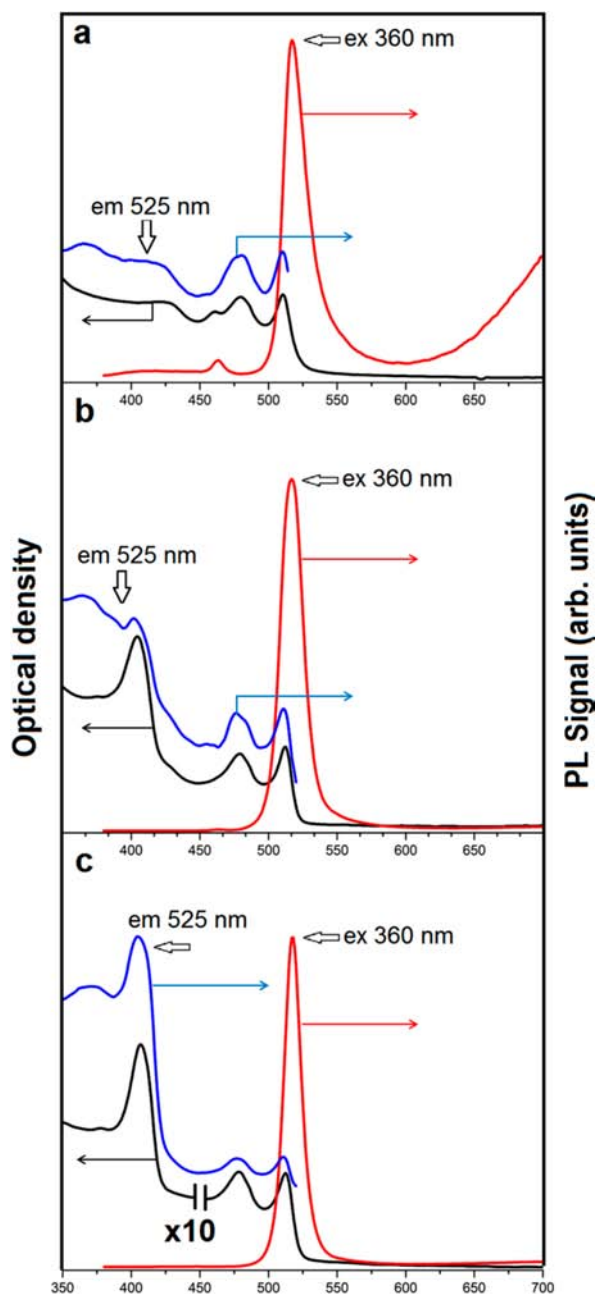


**Figure 1.** Photoluminescence (red curves), optical absorption (black curves), and photoluminescence excitation (blue curves) spectra in chloroform of bare CdSe NPLs (a) and at the intermediate (b) and final (c) stages of CdS overgrowth.  $\lambda_{\text{PL ex}} = 360 \text{ nm}$ ,  $\lambda_{\text{PLE em}} = 525 \text{ nm}$ . The left part of the absorption spectrum in (c) is 10 $\times$  scaled down for visibility.

formation of a nanoheterogeneous structure with efficient charge or energy transfer.

The observed optical effects were in strict contradiction to what was obtained for CdSe NPLs capped with CdS shell.<sup>9,10</sup> In refs 9 and 10, the authors demonstrated that the formation of an epitaxial CdS shell atop a CdSe platelet core resulted in a ca. 100 nm red shift of absorption and PL bands due to changes in the confinement regime. However, in our experiments, we obtained only a 2 nm red-shift after CdS overgrowth. Therefore, we may assume that we grew here something other than an epitaxial CdS shell atop a CdSe NPL core. Figure 2 shows TEM pictures of our CdSe–CdS nanoparticles.

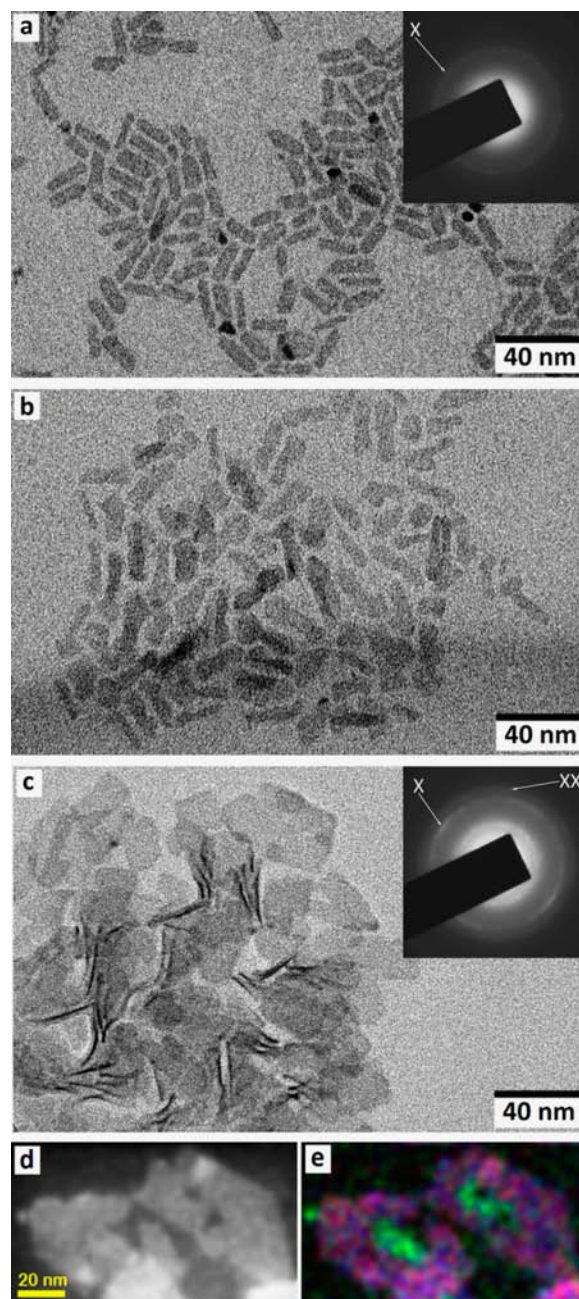


**Figure 2.** TEM images of bare CdSe NPLs (a) and NPLs at the intermediate (b) and final (c) stages of CdS overgrowth. (d) STEM HAADF image of CdSe–CdS NPLs. (e) Color-coded STEM EDX map of corresponding CdSe–CdS NPLs. The red color corresponds to sulfur, green to selenium, and blue to Cd. Individual maps are provided in the Figure S5. Note that images a–c correspond to spectra a–c in Figure 1. Insets in panels a and c show electron diffraction patterns from corresponding nanoparticles. The ring labeled X was assigned to diffraction from the {220} crystalline planes of zinc-blende CdSe; ring XX to diffraction from {222} planes of zinc-blende CdS.

Figure 2a shows bare CdSe NPLs before CdS overgrowth. The lateral size and rectangular shape of CdSe NPLs are similar to those observed earlier in other reports. Figure 2b demonstrates unambiguously the increase in the lateral size of NPLs during the CdS overgrowth. In Table 1 we summarized the data on the lateral size of nanoparticles at the different stages of overgrowth.

**Table 1. Average Lateral Sizes of NPLs at the Different Stages of CdS Overgrowth**

Figure 2 panel	average length (nm)	average width (nm)	average length-to-width ratio
a	19 ± 3	6 ± 1	3.17
b	24 ± 4	7 ± 1	3.43
c	35 ± 6	18 ± 5	1.95

At the beginning of the reaction, CdS grows mostly at the tips of CdSe NPLs, resulting in the increased length-to-width ratio. At the end of the overgrowth process, the lateral size of NPLs has increased approximately twice and final NPLs are less extended and more squared in shape. We may conclude that our experimental conditions provoke the formation of CdSe–CdS nanoheteroplatelets with a CdSe flat core surrounded by CdS flat branches grown at the CdSe platelet edges. Indeed, the elemental mapping of two separate CdSe–CdS NPLs presented in Figure 2e proves the existence of a Se-containing core surrounded by a S-containing region. In such a case the thickness of the CdS branches should be equal to the thickness of the initial CdSe core NPL. Indeed, if we compare the energy of the newly appearing absorption band in Figure 1c with the reported spectral properties of colloidal CdS NPLs, we may see that absorption bands at  $\lambda = 410$  and 510 nm correspond to CdS and CdSe NPLs of equal thickness, respectively.<sup>4</sup> This correlation points to the epitaxial character of CdS grown in the form of flat wings.

Insets in Figure 2a,c show electron diffraction patterns from corresponding regions of TEM images. The pattern X has been assigned to a diffraction from the {220} crystalline planes of the zinc-blende CdSe phase. We detected the appearance of the new pattern XX after CdS overgrowth, and we assigned it to a diffraction from the {222} crystalline planes of the zinc-blende CdS phase (large-scale electron diffraction images can be found in Figures S3 and S4). This is consistent with the results of HRTEM imaging of CdSe–CdS nanoheteroplatelets (see Figure S4). Indeed, we see tilted crystalline planes at the edges of overgrown NPLs. Similar crystalline structure of CdS edges was observed earlier for 1.8 nm thick CdS discs synthesized by colloidal chemistry, having an absorption band also around  $\lambda = 410$  nm.<sup>11</sup> We obtained ca. 5% compression of the CdSe crystalline structure along the  $\langle 220 \rangle$  direction, which follows from the increased diameter of electron diffraction pattern X in Figure 2c as compared to Figure 2a. Figures 2c and S4 also show noticeable bending of NPLs after CdS overgrowth. The differences in the crystalline lattice parameters of zinc-blende CdSe and CdS result in strong mechanical stress in CdSe–CdS nanoheteroplatelets.

XRD analysis of CdSe and CdSe–CdS NPLs powders (Figure S6) confirms that both CdSe and CdS phases have zinc-blende structure. The appearance of a sharp peak from the {200} planes of zinc-blende CdS in CdSe–CdS NPLs may argue for a similar morphology of the CdS wings and CdSe core: both have the largest lateral direction along the  $\langle 200 \rangle$  axis.<sup>11</sup> This result additionally points to the epitaxial character of the CdS wings' growth.

It is logical to assume that the chemical mechanism for the formation of CdS wings is the same as for the formation of the CdSe NPL core. There are two mechanisms explaining the formation of 2D NPLs: oriented attachment of magic-size clusters, discussed in ref 2, or seed-mediated layer-by-layer epitaxial growth.<sup>11</sup> Based on the results in ref 11, we believe

that the last mechanism dominates here. Another question is why CdS forms epitaxial wings in our experiments instead of a full epitaxial shell. The reason for the epitaxial growth of flat CdS wings instead of a CdS shell probably lies in a combination of two factors: relatively high concentration of acetate species in the form of cadmium acetate added to the reaction mixture prior to the CdS overgrowth, and use of short-chain 2-ethylhexanoic acid salt as a cadmium precursor. Instead, long-chain cadmium oleate was used in ref 10 to achieve epitaxial growth of a CdS shell. The long-chain acid may block the epitaxial growth at CdSe edges, provoking isotropic growth of the CdS shell, similar to the well-established procedure for CdSe/CdS core–shell QDs.<sup>12</sup> Another critical parameter which can provoke CdS to grow as wings instead of a shell is the chemical reactivity of precursors for sulfur. We used the less reactive S-ODE complex instead of highly reactive TMS, sulfides, or thioacetamide.<sup>9,10</sup> We suppose that Cd salt does not react with S-ODE complex at the basal {200} plane of CdSe NPLs capped with fatty acids, but easily reacts at the edges of CdSe NPLs probably terminated by {220} crystalline planes. A detailed investigation of the mechanism for 2D growth of epitaxial wings will be the topic for further extended work.

Comparing the PL spectra of bare CdSe and CdSe–CdS NPLs in Figure 1, we see that, besides strong band edge emission, bare CdSe platelets show broad, intense emission in the NIR range which probably belongs to the surface defects. However, the formation of epitaxial CdS wings eliminates the NIR band, which likely points to the localization of surface defects at the edges of CdSe NPLs.

The efficient PL excitation of the CdSe core through photon absorption by CdS wings, which follows from the PLE spectra in Figure 1c, indicates formation of a strongly electrically conjugated structure. Photogenerated electron–hole pairs pass from the CdS wings to the CdSe core, where they recombine radiatively, just generating CdSe band edge emission. This process is illustrated schematically in Figure 3.

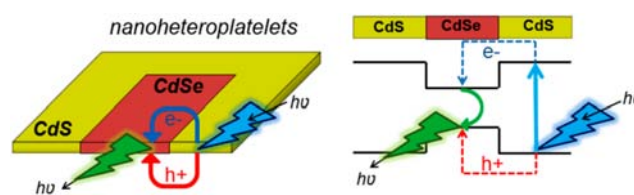


**Figure 3.** Schematic representation of carriers photogeneration in CdS wings, transfer to CdSe nanoplatelet core, and subsequent radiative recombination resulting in CdSe band edge emission. This scheme explains the experimentally observed enhanced CdSe band edge emission when nanoheteroplatelets are excited at the region of CdS absorption.

From Figure 2c–e, we can see that the structure of the CdS wings is highly imperfect. This explains why the magnitude of the PLE band at  $\lambda = 410$  nm in Figure 1c is much less than that of the corresponding absorption band of the CdS wings. At the moment, we are unable to estimate the efficiency of carrier transfer from CdS wings to CdSe core, but it seems to be low due to the imperfection of CdSe–CdS NPLs.

The antenna effect is known and useful for photovoltaic applications (see, for example, refs 13 and 14). CdSe/CdS core–shell NRs synthesized earlier are exciting examples of 1D semiconductor nanoheterostructure with photon antenna effect similar to that of 2D CdSe–CdS nanoheteroplatelets. However,

the extraction of photogenerated carriers from the CdSe core surrounded by CdS antennas in CdSe/CdS NRs can be less efficient as compared to that with CdSe–CdS nanoheteroplatelets, since in the last case both core and antenna are available for creation of electric contacts. Further efforts should be concentrated on the preparation of type II nanoheteroplatelets with intrinsic electron–hole separation between core and antenna.

In conclusion, we demonstrate a novel quantum-confined nanoheterostructure based on a CdSe core nanoplatelet with epitaxially grown flat CdS branches or wings at the CdSe edges. Such a nanoheterostructure shows enhanced optical absorption and PL excitation at the spectral region of CdS absorption. The CdS-mediated photoexcitation of CdSe emission points to efficient charge transfer from the CdS wings into the central CdSe region, which may be utilized in advanced photovoltaic structures. CdS wings may play the role of a photonic antenna to the central CdSe region. Additionally, the extremely high surface area of NPLs allows for efficient physical contact between each individual NPL and conducting polymers in the polymer-based photovoltaic structures, which may sufficiently improve the extraction of photogenerated charge and the total electrical output of the photovoltaic structure. However, much work must be done in order to implement NPLs into real photovoltaic structures. Oleic acid, used as a stabilizer of colloidal NPLs, must be replaced at the surface with shorter molecules allowing for good electric conductivity, similarly to CdSe QDs.<sup>15</sup> However, short-chain stabilizers should provoke strong stacking of NPLs. A combined procedure may be used when the ligand exchange will be done in the presence of a conducting polymer in the colloidal solution of NPLs.

## ■ ASSOCIATED CONTENT

### 📄 Supporting Information

Detailed experimental procedures, additional HRTEM pictures, and electron diffraction data. This material is available free of charge via the Internet at <http://pubs.acs.org>.

## ■ AUTHOR INFORMATION

### Corresponding Author

[m\\_artemyev@yahoo.com](mailto:m_artemyev@yahoo.com)

### Notes

The authors declare no competing financial interest.

## ■ ACKNOWLEDGMENTS

M.A. acknowledges partial funding from the “CHEMRE-AGENTS” Program. A.P. acknowledges partial funding from X13M-017 grant.

## ■ REFERENCES

- (1) Ithurria, S.; Dubertret, B. *J. Am. Chem. Soc.* **2008**, *130*, 16504–16505.
- (2) Ithurria, S.; Bousquet, G.; Dubertret, B. *J. Am. Chem. Soc.* **2011**, *133*, 3070–3077.
- (3) Li, Z.; Peng, X. *J. Am. Chem. Soc.* **2011**, *133*, 6578–6586.
- (4) Ithurria, S.; Tessier, M. D.; Mahler, B.; Lobo, R. P. S. M.; Dubertret, B.; Efros, A. L. *Nat. Mater.* **2011**, *10*, 936–941.
- (5) Achtstein, A. W.; Schliwa, A.; Prudnikau, A.; Hardzei, M.; Artemyev, M. V.; Tjomsen, C.; Woggon, U. *Nano Lett.* **2012**, *12*, 3151–3157.
- (6) Cassette, E.; Mahler, B.; Guigner, J.-M.; Patriarche, G.; Dubertret, B.; Pons, T. *ACS Nano* **2012**, *6*, 6741–6750.

(7) Pelton, M.; Ithurria, S.; Schaller, R. D.; Dolznikov, D. S.; Talapin, D. V. *Nano Lett.* **2012**, *12*, 6158–6163.

(8) Tessier, M. D.; Javaux, C.; Maximovic, I.; Loriette, V.; Dubertret, B. *ACS Nano* **2012**, *6*, 6751–6758.

(9) Ithurria, S.; Talapin, D. V. *J. Am. Chem. Soc.* **2012**, *134*, 18585–18590.

(10) Mahler, B.; Nadal, B.; Bouet, C.; Patriarche, G.; Dubertret, B. *J. Am. Chem. Soc.* **2012**, *134*, 18591–18598.

(11) Li, Z.; Qin, H.; Guzin, D.; Benamara, M.; Salamo, G.; Peng, X. *Nano Res.* **2012**, *5*, 337–351.

(12) Samokhvalov, P.; Artemyev, M.; Nabiev, I. *Chem.—Eur. J.* **2013**, *19*, 1534–1546.

(13) Mamedova, N. N.; Kotov, N. A.; Rogach, A. L.; Studer, J. *Nano Lett.* **2001**, *1*, 281–286.

(14) Talapin, D. V.; Nelson, J. H.; Shevchenko, E. V.; Aloni, S.; Sadtler, B.; Alivisatos, A. P. *Nano Lett.* **2007**, *7*, 2951–2959.

(15) Nag, A.; Kovalenko, M. V.; Lee, J.-S.; Liu, W.; Spokoyny, B.; Talapin, D. V. *J. Am. Chem. Soc.* **2011**, *133*, 10612–10620.